Optics and Lasers in Engineering 151 (2022) 106932

Contents lists available at ScienceDirect

Optics and Lasers in Engineering

journal homepage: www.elsevier.com/locate/optlaseng

Unbalanced low coherence interference microscopy

Azeem Ahmad*, Anowarul Habib, Vishesh Dubey, Balpreet Singh Ahluwalia

Department of Physics and Technology, UiT The Arctic University of Norway, Tromsø, Norway

ARTICLE INFO

Keywords:
Low coherence interferometry
Quantitative phase microscopy
Interference microscopy
Optical metrology
Biomedical imaging

ABSTRACT

Low coherence interference microscopy (LCIM) provides high spatial phase sensitivity, i.e., speckle free and coherent noise free quantitative phase images of the test specimens. Due to low temporal coherence (TC) length of the light source, LCIM requires precise adjustment of the optical path difference (OPD) between the object and the reference arm, which is only a few micrometers. Consequently, previously demonstrated LCIM systems are implemented with the use of identical objective lenses in both the arms and also known as balanced interferometric configuration. The use of identical objective lens hinders both the use of high numerical aperture objective lens and also the swift change of the objective lens during imaging. In the present work, LCIM is implemented with non-identical objective lenses in the object and the reference arm also called unbalanced optical configuration. A range of objective lenses 10 × /0.25NA, 20 × /0.45NA and 60 × /1.2NA are employed in the object arm of the system while keeping single objective lens 10 × /0.25NA in the reference arm. To resolve the challenges associated with unbalanced configuration, advanced iterative algorithm (AIA) and principal component analysis (PCA) algorithms are integrated to recover quadratic phase error free phase images of the test specimens. The capabilities of the proposed method are exhibited on various specimens like USAF resolution, step-like test object and for the biological cells, HeLa cells. The proposed approach enables scalable magnification and resolution by simply rotating the imaging objective turret without the need of changing objective lens in the reference arm.

1. Introduction

Low coherence interference microscopy (LCIM) also known as white light interference microscopy is a widely accepted technique in the field of optical profilometry, quantitative phase microscopy and full field optical coherence tomography (FFOCT) [1–6]. In optical profilometry, LCIM allows extended range of height measurement, which is not possible in monochromatic light source, i.e., laser-based interferometry systems [7–10]. In FFOCT, low coherent light sources are utilized to generate three dimensional optical images of the specimens with high axial resolution depending on the temporal coherence length of the light source [4,11]. The three-dimensional optical images of the specimens can also be obtained by employing high numerical aperture objective lenses. Here, the axial resolution is decided by the longitudinal spatial coherence length, i.e., depth of field, rather than the temporal coherence length of the light source [12].

LCIM utilizes the spectrally broad band light sources like halogen lamp, super luminescent diodes and light emitting diodes (LEDs) to form the interference pattern at the detector plane. The use of these light sources imposes a constraint on optical path difference (OPD) adjustment within their short TC length, which is done by employing identical objective lenses in both the object and the reference arm of LCIM in the past [4,5]. This is also called balanced optical configuration. In addition, the low TC property of the white light (WL) source leads to the formation of speckle noise free, coherent noise free, and parasitic fringe free interferometric images of the specimens [3,13]. Thus, it generates superior quality images of the specimens under study. Moreover, it provides accurate quantitative height/phase maps of the ultrathin specimens as well which are otherwise difficult to image with the high TC length light sources like lasers [2,14]. However, this comes with a cost of more precise optical alignment, due to the need of OPD adjustment within the TC length of the light source. In addition, WL source generates limited interference field of view (FOV) at the camera [15]. Therefore, it is good to use relatively narrow spectral bandwidth light sources like LEDs or filtered white light (FWL) rather than pure WL source in the LCIM system.

The LEDs or FWL sources are also partially temporally coherent and have couple of micrometer TC length depending on their spectral bandwidths. Thus, in the past identical objective lenses have been used in both the object and the reference arm of the LCIM systems based on Linnik and Mach-Zehnder interferometric configurations [4,16]. The use of identical objective lenses in both the arms of interferometer limits the

* Corresponding author.
E-mail addresses: ahmadazeem870@gmail.com (A. Ahmad), balpreet.singh.ahluwalia@uit.no (B.S. Ahluwalia).

https://doi.org/10.1016/j.optlaseng.2021.106932
Received 9 May 2021; Received in revised form 10 September 2021; Accepted 19 December 2021
Available online 3 January 2022

applicability of the system, as a change in the imaging objective lens would require changing the objective lens at the reference arms as well. This problem is usually avoided by pre-defined use of an imaging and reference objective lenses, but is then devoid of flexibility in imaging magnification and resolution. Furthermore, the problem is more challenging while working with immersion objective lenses to obtain higher resolution. It is cumbersome to use the immersion objective lens in the reference arm as it increases instability and complexity in the system. Mirau interferometer is another kind of interference microscopy configuration which is also used to obtain interference pattern quickly with WL source [1,2,17,18], however, it has a limited highest possible transverse resolution corresponding to 0.7 numerical aperture (N.A.) and fixed reference arm.

The focus of the present work is the implementation of low TC light source in LCIM having non-identical objective lenses in the object arm and the reference arm. This opens the flexibility to achieve scalable FOV and resolution in LCIM system, which is not done previously. Here, Linnik interference microscopy system is implemented with unfiltered WL and FWL for a range of imaging objective lenses in the object arm and a single objective lens in the reference arm. The reference arm of the interferometer always has 10 × /0.25NA objective lens, whereas, in the object arm 10 × /0.25NA, 20 × /0.45NA and 60 × /1.2NA objective lenses are sequentially inserted to acquire scalable FOV and resolution. The phase recovery of the specimens is done by implementing advanced iterative algorithms (AIA) which requires phase shifted interferograms and has the capability to recover quantitative phase maps from the randomly phase shifted interferograms [19].

First, the effect of non-identical objective lenses on the performance of LCIM in terms of spatial phase sensitivity is systematically studied. As different objective lenses have different amount of optical dispersion, therefore, its effect is systematically studied by utilizing pure WL and FWL generated by inserting different bandpass filters of spectral bandwidths 69, 10, and 3 nm in LCIM. In addition, the use of non-identical objective lenses in the interferometer enforces the adjustment of the OPD between both arms, the object and the reference, within the TC length of the light source to obtain interference pattern. The OPD adjustment is done by translating the reference arm (objective + mirror). The OPD adjustment for non-identical objective lenses is done at the cost of non-equal geometrical path lengths of the object and the reference arms. This leads to the generation of circular fringes instead of straight fringes in the interference microscopy system due to the wavefront curvature mismatch in both arms of LCIM. Consequently, it generates an unwanted quadratic phase error in the recovered phase images. The quadratic phase error is compensated by employing principle component analysis (PCA) algorithm which is only implemented for the single shot phase recovery algorithm in the past [20]. The implementation of PCA method with phase shifting recovery algorithm is absent from the literature. Thus, the integration of AIA and PCA algorithms allow quadratic aberration free phase recovery of the specimens corresponding to different objective lenses using unbalanced LCIM. Note that the proposed approach is not restricted only to AIA and PCA algorithms and can be implemented with any other phase recovery and compensation algorithm. The use of low TC light source in interference microscopy system and above algorithms during reconstruction leads to the formation of high resolution, quadratic phase error free and highly spatial phase sensitive quantitative phase images of the test specimens.

2. Material and methods

2.1. Mathematical description

The 2D modulated intensity of the interferograms can be expressed as follows [19]:

$$I_m(x,y) = A_m(x,y) + B_m(x,y)\cos\left[\phi(x,y) + \delta_m\right] \quad (1)$$

where, subscript m represents the mth phase shifted interferogram (m = 1,2,3,…, M). $A_m(x,y)$ is the background, $B_m(x,y)$ is the modulation amplitude, $\phi(x,y)$ is the phase of the test object with respect to the outside media and δ_m is the amount of phase shift between the consecutive interferograms. Let us assume N is the total number of pixels in the individual interferogram.

Under the assumption that $A_m(x,y)$ and $B_m(x,y)$ don't have frame by frame variation, define a new set of variable $a(x,y) = A_m(x,y)$, $b(x,y) = B_m(x,y)\cos\phi_n$ and $c(x,y) = -B_m(x,y)\sin\phi_n$. The Eq. (1) can be rewritten as follows:

$$I_m(x,y) = a(x,y) + b(x,y)\cos\delta_m + c(x,y)\sin\delta_m \quad (2)$$

With known δ_m,there are 3 N unknowns and MN equations. These unknowns can be solved by employing AIA algorithm [19] and the phase can be obtained by the following expression:

$$\phi(x,y) = \tan^{-1}\left[-c(x,y)/b(x,y)\right] \quad (3)$$

The complex field associated with the phase '$\phi(x,y)$' can be expressed as follows:

$$U(x,y) = \exp\left[i\phi(x,y)\right] \quad (4)$$

If the recovered phase has linear and quadratic aberration terms, then the above Eq. (4) can be written as:

$$U(x,y) = \exp\left[i\phi(x,y)\right]Q(x,y) \quad (5)$$

where, $Q(x,y)$ is the aberration term and defined as follows [20]:

$$Q(x,y) = \exp\left[i\left(k_x x + k_y y\right)\right]\exp\left[i\left(l_x x^2 + l_y y^2\right)\right] \quad (6)$$

where, k_x and k_y represent the linear phase difference between the object and reference beam and is arises due to the angle between them. The parameters l_x and l_y describe the relative divergence between the object and the reference beams due to their wavefront curvature mismatch.

The phase aberration term '$Q(x,y)$' defined in Eq. (6) is compensated by employing PCA approach [20], which effectively remove this type of phase error from the recovered phase maps.

2.2. Experimental setup

The experimental scheme of LCIM system is illustrated in Fig. 1 and works on the principle of Linnik based interference microscopy system. The light coming from a white light source (halogen lamp) is coupled into a multi-mode fiber (MMF) of 1 mm core diameter using a coupling lens CL_2. This improves the spatial coherence length of the white light source. The TC length of the WL source is increased by inserting a spectral bandpass filter into the light beam path at the output of MMF. This is required to achieve high contrast interference fringes over the whole camera FOV while working with non-identical objective lenses. The narrow bandwidth of the filtered white light (FWL) alleviates the problem of optical dispersion while working with high NA objective lenses. For spatial phase sensitivity comparison, a laser light beams coming from a diode laser (λ = 638 nm; $\Delta\lambda$ = 0.1 nm) is coupled into a single-mode fiber (SMF) using a coupling lens CL_1. The output of SMF generates temporally and spatially high coherent light beam.

The output port of MMF and SMF is attached with the input port of interference microscopy system as illustrated in Fig. 1. The light beams coming from SMF and MMF are combined using beam splitter BS_1. The combination of lenses L_1 (fl = 75 mm) and L_2 (fl = 125 mm) relay the source image at the back focal plane of the microscope objective MO_2 to achieve uniform illumination at the sample plane. Here, a range of objective lenses 10 × /0.25NA, 20 × /0.45NA and 60 × /1.2NA are used in the object arm to achieve user defined magnification and resolution. The beam splitter BS_2 split the input beams into two; one is directed towards the sample (S) and the other one towards reference objective lens (MO_1) and mirror (M). The reference objective lens is always kept 10 × /0.25NA during the whole experimentation. The light beams reflected from the sample and M recombine and forms interference pattern

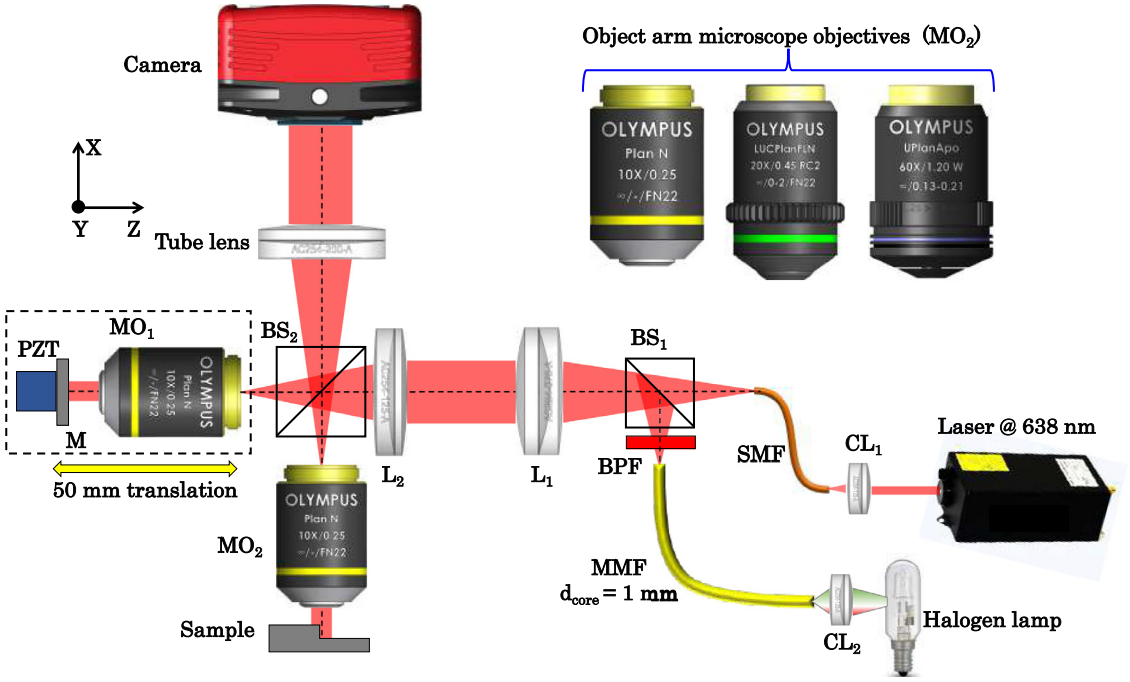

Fig. 1. Schematic diagram of LCIM system. MO_{1-2}: Microscope objectives; BS_{1-2}: Beam splitters; L_{1-2}: Achromatic doublet lenses; CL_{1-2}: Coupling lenses; BPF: Bandpass filter; MMF: Multi-mode fiber; SMF: Single mode fiber; M: Mirror and PZT: Piezo electric transducer.

at the same beam splitter plane, which is projected at the camera plane with the help of tube lens (fl = 180 mm) to form interference pattern.

As the reference objective lens is fixed, therefore, MO_1 and mirror are attached to a long travel range motorized linear translation stage (50 mm) to adjust the OPD between the object and reference arm of LCIM. This is required to obtain interference patterns while switching different MO_2 in the object arm for achieving scalable FOV and resolution. The reference mirror M is attached to a piezo stage to introduce temporal phase shift between the object and reference arm with nanometer precision. The piezo stage and high-speed complementary metal oxide semiconductor (CMOS) camera are synchronized using micromanager to record phase shifted interferograms. Further, the phase shifted interferograms of the test objects are used to retrieve their diffraction limited phase maps as illustrated in the forthcoming sections.

3. Results and discussion

3.1. Optical path difference measurement for different objective lenses

In the present LCIM system, reference arm always has 10 × /0.25 objective lens, and in the object arm different objective lenses are used 10 × /0.25, 20 × /0.45 and 60 × /1.2 NA. The optical path lengths of non-identical objective lenses are not equal and generates different OPD between both arms of the system. Therefore, in order to achieve interference fringes with low TC length light source for all objective lenses, the OPD must be adjusted and bring within the TC length. It is done by translating the reference arm (objective + mirror) and continuously observing the formation of interference fringes at the detector. First, the zero OPD position is achieved by using identical objective lenses (10 × /0.25) in both arms. It forms straight fringes at zero OPD position. The reference arm (objective + mirror) is then translated to adjust the OPD within TC length for other objective lenses 20 × /0.45 and 60 × /1.2 NA to achieve interference fringes. This leads to the formation of curved fringes instead of straight fringes due to the wavefront curvature mismatch between the object and the reference beam at zero OPD position. The OPDs are measured to be equal to 9.94 mm and 27.62 mm for 20 × /0.45 and 60 × /1.2 NA, respectively.

3.2. Effect of optical dispersion due to non-identical objective lenses in LCIM

As different objective lenses have different optical dispersion, therefore, it becomes important to understand its effect on the performance of LCIM as a function of the spectral bandwidth of the light source. The use of non-identical objective lenses introduces the problem of uncompensated dispersion/chromatic aberration in the images which reduces the fringe contrast significantly. The problem of dispersion/chromatic aberration is systematically studied by utilizing pure WL and FWL generated by inserting different bandpass filters at central wavelength/spectral bandwidths: 630 nm/69 nm, 632 nm/10 nm, and 632 nm/3 nm in LCIM.

The experiment is conducted with water immersion objective lens 60 × /1.2NA in the object arm and 10 × /0.25NA in the reference arm. Fig. 2a–d illustrate the full FOV interference fringes corresponding to unfiltered WL and FWL (630/69 nm; 632/10 nm; and 632 nm/3 nm). The zoomed views of the regions marked with yellow color solid boxes are exhibited in Fig. 2e–h. The interference signals are normalized by dividing from their maximum values and displayed in the range 0 to 1 for clearly demonstrating the effect of optical dispersion on their fringe contrast. It can be seen that the use of WL and FWL at 630/69 nm in LCIM reduces the fringe contrast significantly due to uncompensated dispersion as depicted in Fig. 2e and f. This will further reduce the spatial phase sensitivity of the system as illustrated in Fig. 2i and j. On the contrary, the fringe contrast is observed to be quite high for FWL at 632/10 nm and 632/3 nm as shown in Fig. 2g and h. Thus, narrow bandpass filters reduce the effect of dispersion and reconstruct the phase images of the targeted specimen with significantly reduced phase noise as presented in Fig. 2k and l. Similar studies are performed and found to be same for other objective lenses 20 × /0.45NA and 60 × /0.7NA in the object arm keeping 10 × /0.25NA in the reference arm, which are not included here. It is observed that bandpass filter of 10 nm bandwidth or smaller is sufficient to provide high contrast interference fringes over

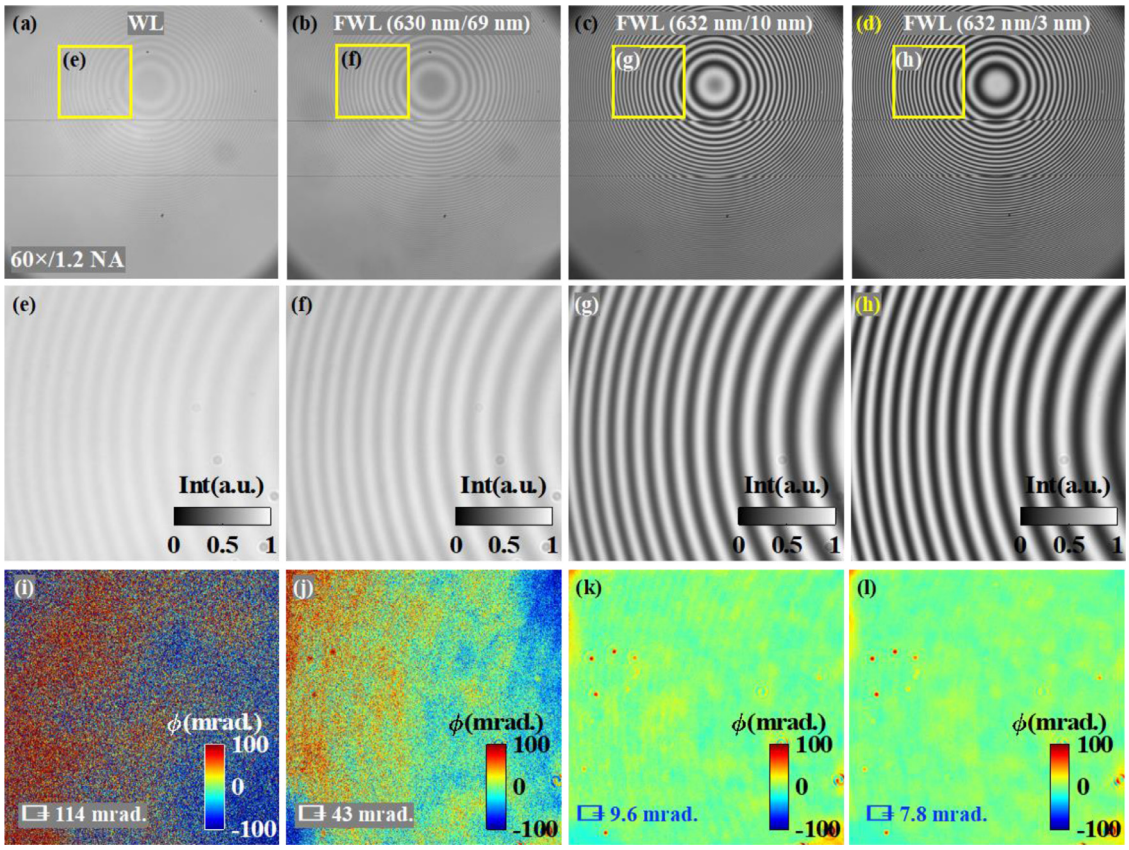

Fig. 2. (a–d) Full FOV interference signal corresponding to unfiltered white light and filtered white light at peak wavelength with spectral bandwidth 630/69 nm, 632/10 nm, and 632 nm/3 nm. (e–h) Zoomed views of the region marked with yellow color solid boxes. (i–l) Reconstructed phase maps to illustrate the influence of optical dispersion on the spatial phase sensitivity of LCIM system.

the whole FOV of the camera and subsequently reduction in the spatial phase noise of unbalanced LCIM system significantly.

3.3. Quadratic aberration free diffraction limited phase reconstruction

In order to exhibit the capability of the phase reconstruction (AIA) and quadratic phase error compensation (PCA) algorithm, the experiment is conducted on a USAF resolution test target (Newport: model # RES-1). For AIA reconstruction algorithm, 10 phase shifted interferograms within a range of 0–2π are recorded. One of the phase shifted interferograms of USAF chart is depicted in Fig. 3a. The interferograms are recorded with 20 × /0.45 NA objective lens. It can be seen that the shape of the fringes is curved instead of straight fringes due to the use of non-identical objective lenses in both arms of the interferometer as explained in the last section.

The wrapped phase map obtained from AIA algorithm is shown in Fig. 3b. The wrapped phase map is then unwrapped using phase unwrapping algorithm [21] and presented in Fig. 3c. It can be visualized that the recovered phase map has quadratic phase aberration error due to the curved interference fringes. This quadratic phase aberration is then compensated by employing PCA method. It can also be compensated by recording and subtracting the reference phase corresponding to the reference interferograms at the cost of less temporal resolution as presented in the next section. The compensated phase map of the USAF chart is illustrated in Fig. 3d. It can be visualized from Fig. 3d that the compensated phase map still has slowly varying background phase, which is due to the presence of other optical aberrations like spherical, field flatness and distortion etc. in the system. The reconstructed phase map does not suffer from the coherent noise due to the use of low TC length light source.

3.4. Phase error analysis

In order to perform this study, we compared PCA compensated phase with the standard double exposure method. In double exposure method, two interferograms are required one with sample (object interferogram) and other without sample (reference interferogram). The corresponding recovered phase maps are then subtracted for quadratic phase aberration compensation. The experiments are performed using 20 × /0.45 NA objective lens on a standard object, i.e., step/barrier like structure. The structures are made on a Si wafer and fabricated by etching the Si wafer down to approximately 110 nm depth. For double exposure method, the phase shifted object interferogram and the reference interferograms corresponding to structure free flat region on the sample are recorded and analyzed for phase recovery. One of the phase shifted reference and object interferograms and corresponding recovered wrapped phase maps are illustrated in Fig. 4a–d. The phase recovery from object and reference interferograms is done by using AIA algorithm. The wrapped phase maps are then unwrapped using minimum Lp norm phase unwrapping algorithm. The unwrapped phase map corresponding to reference interferogram is subtracted from the object unwrapped phase map to obtain quadratic aberration free phase images. The subtracted phase map of step like structure is presented in Fig. 4e. Next, quadratic phase aberration error from the object phase map is compensated numerically using PCA algorithm. The compensated phase map is shown in Fig. 4f. For error analysis, PCA compensated phase map is subtracted from the double exposure compensated phase map and illustrated in Fig. 4g. The phase

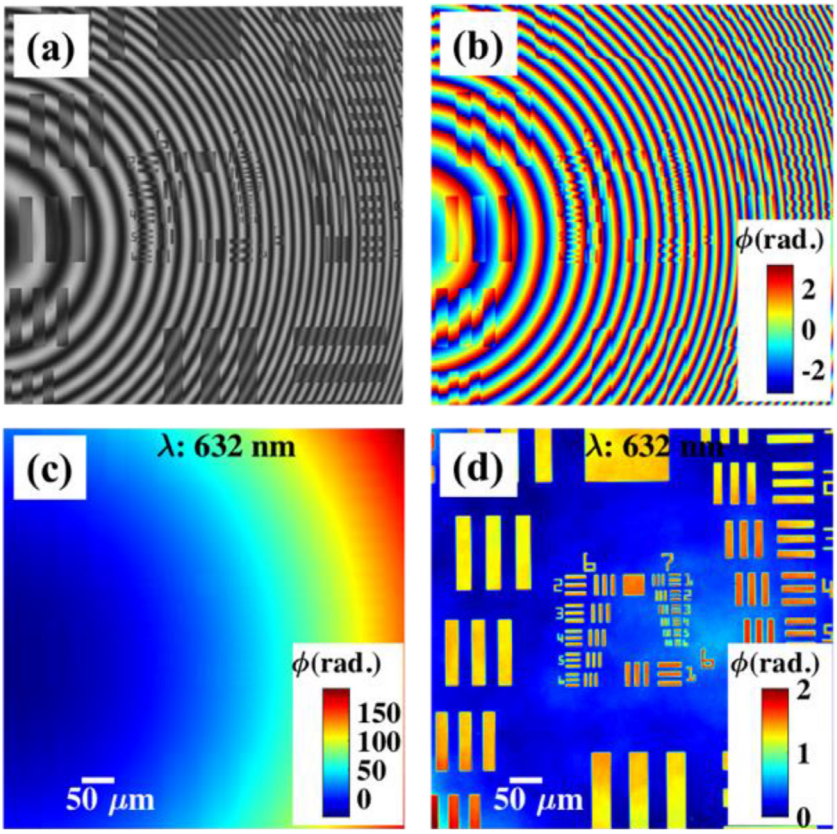

Fig. 3. Quadratic aberration free phase reconstruction. A bandpass filter of 3 nm spectral bandwidth at central wavelength 632 nm is inserted into the white light beam path to generate FWL. (a) One of the phase shifted interferograms of USAF chart recorded with 20 × /0.45 NA objective lens. (b) Wrapped phase map obtained by employing AIA phase recovery algorithm. (c) Unwrapped phase map without the removal of unwanted quadratic phase error which is generated due to the curved fringes. (d) PCA compensated unwrapped phase map. The color bars are in rad.

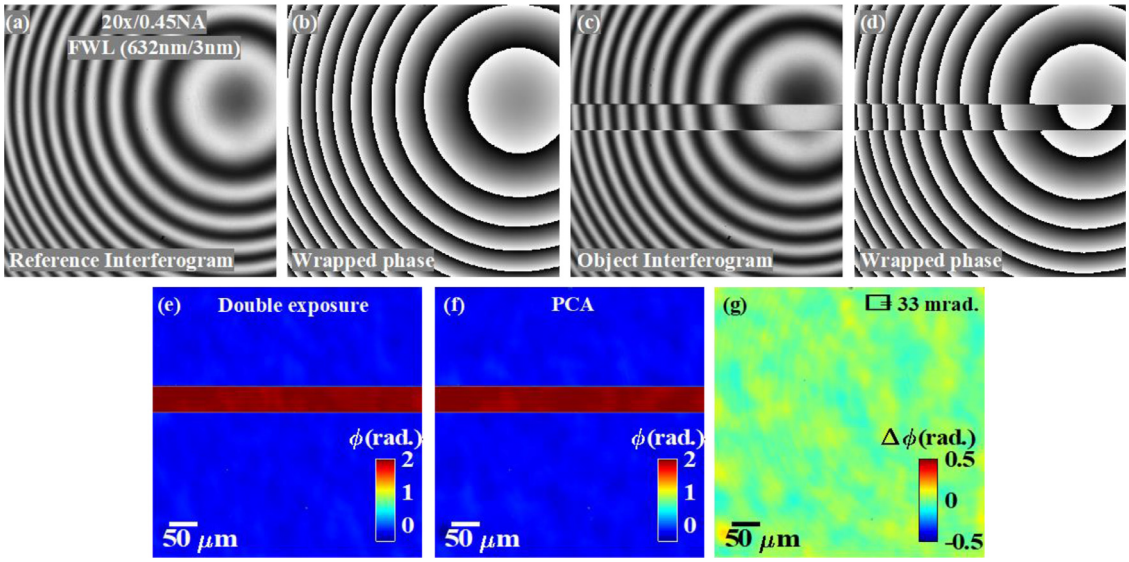

Fig. 4. (a, c) Reference and object interferogram recorded using 20x/0.45NA objective lens and bandpass filter at peak wavelength of 632 nm with 3 nm spectral bandwidth. (b, d) Corresponding wrapped phase maps retrieved by employing AIA. (e, f) Quadratic aberration compensated phase maps corresponding to double exposure based physical method and PCA based numerical method, respectively. (g) Error phase map between the compensated phase maps for double exposure and PCA based approach.

error is measured to be equal to 33 mrad. Thus, compensated phase maps are found to be in a good agreement with each other.

3.5. Comparison of laser vs FWL based phase reconstruction

To compare the capability of LCIM while working with FWL and laser, the experiments are conducted on a standard Si wafer having structures of approximately 110 nm height. The specimen is placed under the LCIM (Fig. 1) to acquire random phase shifted interferograms corresponding to direct laser and FWL both as depicted in Fig. 5(a) and 5(d), respectively. It can be visualized in Fig. 5(a), diode laser interferogram suffers from the coherent noise generated due to high temporal and spatial coherence length of the laser. In contrast, FWL produces coherent and speckle noise free interferogram as illustrated in Fig. 5(d). The data is recorded with 20 × /0.45 NA objective lens. The recorded interferograms are further post-processed by employing AIA and PCA

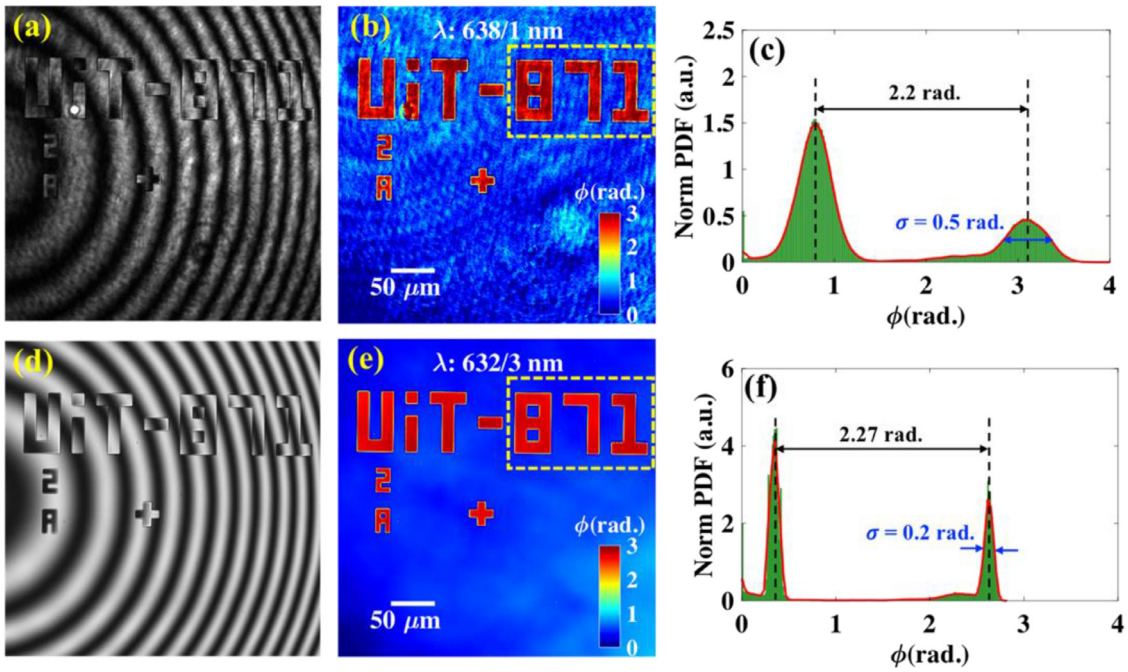

Fig. 5. FWL prevents coherent noise formation. A bandpass filter of 3 nm bandwidth at central wavelength 632 nm is inserted into the white light beam path to generate FWL. (a, d) One of the phase shifted interferometric images of a UiT text fabricated by etching Si wafer. (b, e) Corresponding reconstructed phase images while employing laser and FWL, respectively. (c, f) Normalized probability density functions of the region marked with yellow dotted box in the recovered phase images of Si wafer. The FWL effectively suppresses the spatial phase noise in the recovered phase images. The color bars are in rad.

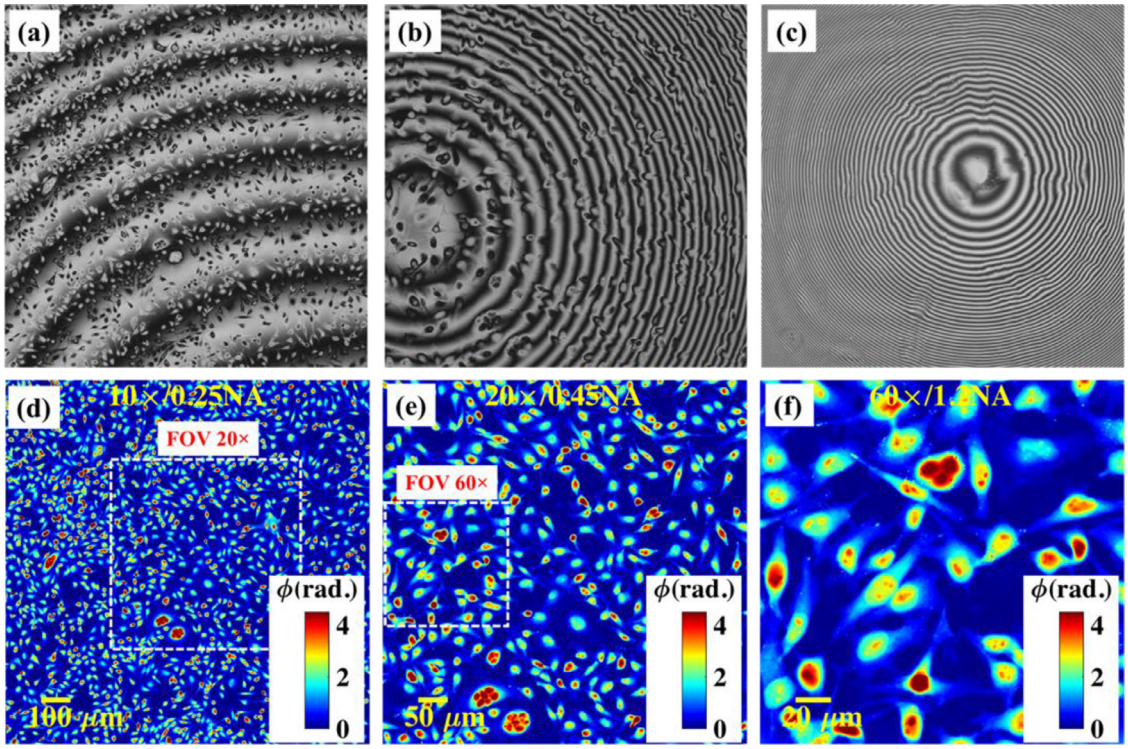

Fig. 6. Scalable FOV and resolution in LCIM. Three objective lenses with different magnification and numerical aperture were used: 10 × /0.25NA, 20 × /0.45NA and 60 × /1.2NA. (a–c) Interferometric images of HeLa cells recorded with FWL while sequentially using 10 × /0.25NA, 20 × /0.45NA and 60 × /1.2NA objective lens in the object arm, respectively. (d–f) Reconstructed phase images of the cells corresponding to aforementioned objective lenses. The white dotted boxes in Fig. 6(d) and (e) exhibit the 20 × and 60 × FOVs. The scale bars are in micron.

algorithms for the quadratic phase error free quantitative phase maps of UiT text fabricated on a Si wafer. Subsequently, the phase maps can be used to measure the height maps of text for both laser and FWL by using $H(x, y) = \lambda\phi(x, y)/4pi$, where λ is the peak wavelength of the light source. Fig. 5(b) and (e) illustrate the reconstructed phase maps of the UiT text corresponding to diode laser and FWL, respectively.

The normalized histogram plots of the region marked with yellow dotted box for both sources are illustrated in Fig. 5(c) and 5(f), respectively. It is observed from the histogram plots that diode laser generates large coherent noise in the recovered phase maps compared to FWL. The phase difference between the structure's foreground and background are measured to be equal to 2.2 rad. and 2.27 rad. for laser and FWL, respectively. It can be seen that the spatial phase noise is large in case of laser compared to FWL. The standard deviation values are measured to be approximately equal to 0.5 rad and 0.2 rad for laser and FWL, respectively. It is quite evident from Fig. 5(c) and (f) that the coherence property of the light source plays an important role in deciding the phase measurement sensitivity of the system. Thus, partially spatial and partially temporal coherent light source, like FWL in the present work, generates superior quality interferometric and subsequently phase images of the specimen. High spatial phase sensitivity is required when minute structures like membrane of liver sinusoidal endothelial cells (H ~100 nm), tail of the sperms and thin optical waveguide are needed to be imaged. These structures would be difficult to image in a laser based interferometric systems.

3.6. Scalable field of view and resolution

The scalable FOV and resolution is indispensable in the LCIM system. It provides the flexibility to the user to acquire, first, the extremely large FOV with low magnification objective lens and then the high-resolution phase images of the region of interest. In the previous sections, it has been demonstrated that non-identical objective lenses can be used in the object and the reference arm of the LCIM system to obtain interference fringes with low TC length light source. In this section, the experiments are conducted on the biological sample (HeLa cells) to exhibit the scalable FOV and resolution capability of the present approach. The data is acquired with three different 10 × /0.25, 20 × /0.45 and 60 × /1.2 NA objective lenses in the object arm of LCIM system. To prepare the sample, first, PDMS chamber having opening area 10 × 10 mm is placed on top of the Si wafer. The HeLa cells are grown in the PDMS chamber and then covered from the top using a 170 μm thick cover glass.

Fig. 6(a)–(c) illustrate one of the phase shifted interferograms of HeLa cells corresponding to 10 × /0.25NA, 20 × /0.45NA and 60 × /1.2NA objective lenses, respectively. It can be seen from the interferograms that the shape of the fringes is circular for all objective lenses. This is due to the wavefront curvature mismatch between the object and the reference beam at zero OPD position while working with 20 × /0.45NA and 60 × /1.2NA objective lenses. The 60 × /1.2NA objective lens generates large curvature mismatch than 20 × /0.45NA objective lens and forms relatively high-density fringes as presented in Fig. 6(b) and (c). For identical objective lenses 10 × /0.25NA in both the object and the reference arm, the shape of the fringes is also circular. In this case, slight curvature mismatch is arising due to the sample, which generated extra OPD in the object beam compared to the reference beam. These interferograms are further post processed to measure the corresponding phase maps using AIA and PCA algorithms. The recovered phase maps of HeLa cells corresponding to 10 × /0.25NA, 20 × /0.45NA and 60 × /1.2NA objective lenses are illustrated in Fig. 6(d)–(f), respectively. It can be visualized that the recovered phase maps do not suffer from the speckle noise and coherent noise. The use of FWL generates highly spatial phase sensitive phase images of the biological specimens over the whole camera FOV. Thus, it demonstrates that the present approach provides the possibility of obtaining scalable FOV and resolution with high spatial phase sensitivity in interference microscopy system.

4. Conclusion and discussion

In the present work, LCIM is implemented with non-identical objective lenses in the object and the reference arm and low TC length (~ 60 μm) light source. LCIM has advantages such as optical sectioning due to the short TC length of the light source, extended range of height measurement in profilometry compared to monochromatic light source-based interferometry system, and generation of three-dimensional images in FFOCT system. Along with these advantages, the use of low TC light source in interference microscopy system significantly increases its phase measurement sensitivity compared to laser.

High spatial phase sensitivity is indispensable in the LCIM system for imaging thin biological specimens like membrane of LSECs [2], tail of sperm, extracellular vesicles, bacteria and liposomes which introduce minute optical lengths in the light wavefront. Such objects are difficult to image under laser-based interference microscopy system due to the coherent noise. The problem of coherent noise can be resolved by employing LCIM system, which utilizes low TC length light sources instead of high TC length light source like laser. At the same time, the low TC length imposes a constraint on the LCIM. This limits the use of only identical objective lenses in both arms of the interference microscopy system. The identical objective lenses do not disturb the zero OPD condition between the object and the reference arm and helps to form the interference fringes even with the low TC length light sources. This overall restricts the applications of LCIM system only for a specific objective lens.

On the contrary, the use of non-identical objective lenses introduces extra OPD (larger than TC length of the light source) and optical dispersion mismatch between the object and the reference field of LCIM system while switching different objective lenses in the object arm and consequently washout the interference fringes. The OPD adjustment is done by translating the reference arm (objective lens + mirror) and optical dispersion compensation is done by employing FWL with spectral bandwidth less than 10 nm. At zero or nearly zero OPD position, the interference fringes again appear at the camera. It disturbs the geometrical path length between the object and the reference arm of the system and introduce wavefront curvature mismatch between the interfering beams. This leads to the formation of curved fringes in place of straight fringes and subsequently introduces an unwanted quadratic phase error in the recovered phase maps.

The AIA algorithm is implemented for the quantitative phase recovery of the test specimens which reconstruct the diffraction limited phase images from the randomly phase shifted interferograms. The quadratic phase error is compensated by employing PCA algorithm, which is implementing only for a single shot phase recovery algorithm in the past. It is demonstrated that these algorithms work effectively in the present unbalanced LCIM system and generates high quality phase images of the specimens without losing any resolution during the reconstruction steps. The capability of the present approach is exhibited by performing phase imaging of the USAF chart, step like object (UiT text) and scalable FOV imaging of HeLa cells. Thus, user defined scalable FOV and resolution can be easily obtained in LCIM system. The present approach would also enable the use of highest possible resolution immersion objective lenses for phase imaging of a variety of specimens. We believe the present approach would have a wide penetration in the field of interference microscopy and opens the avenue for wide range of bio applications in future.

Data and materials availability

The authors declare the availability of the data used in the research to obtain the results reported in the manuscript upon reasonable request.

Declaration of Competing Interest

The authors declare no conflicts of interest.

CRediT authorship contribution statement

Azeem Ahmad: Visualization, Conceptualization, Investigation, Formal analysis, Writing – original draft, Supervision, Writing – review & editing. **Anowarul Habib:** Investigation, Writing – review & editing. **Vishesh Dubey:** Investigation, Writing – review & editing. **Balpreet Singh Ahluwalia:** Writing – original draft, Project administration, Supervision, Writing – review & editing.

Acknowledgments

B.S.A. acknowledges the funding from Research Council of Norway, INTPART project (309802), Nano2021 project (2021–288565) and BioTek Project (2021–285571).

References

[1] Ahmad A, Kumar A, Dubey V, Butola A, Singh Ahluwalia B, Mehta DS. Characterization of color cross-talk of CCD detectors and its influence in multispectral quantitative phase imaging. Opt Express 2019;27(4):4572–89.
[2] Ahmad A, et al. Sub-nanometer height sensitivity by phase shifting interference microscopy under environmental fluctuations. Opt Express 2020;28(7):9340–58.
[3] Bhaduri B, et al. Diffraction phase microscopy with white light. Opt Lett 2012;37(6):1094–6.
[4] Dubois A, et al. High-resolution full-field optical coherence tomography with a Linnik microscope. Appl Opt 2002;41(4):805–12.
[5] Vabre L, Dubois A, Boccara AC. Thermal-light full-field optical coherence tomography. Opt Lett 2002;27(7):530–2.
[6] Dubey V, et al. White light phase shifting interferometry and color fringe analysis for the detection of contaminants in water Quantitative phase imaging ii. International Society for Optics and Photonics; 2016.
[7] Davidson M, et al. An application of interference microscopy to integrated circuit inspection and metrology Integrated circuit metrology, inspection, & process control. International Society for Optics and Photonics; 1987.
[8] Lee BS, Strand TC. Profilometry with a coherence scanning microscope. Appl Opt 1990;29(26):3784–8.
[9] de Groot P, Deck L. Three-dimensional imaging by sub-Nyquist sampling of white–light interferograms. Opt Lett 1993;18(17):1462–4.
[10] Hariharan P, Roy M. White-light phase-stepping interferometry for surface profiling. J. Mod. Opt. 1994;41(11):2197–201.
[11] Roy M, et al. Geometric phase-shifting for low-coherence interference microscopy. Opt. Lasers. Eng. 2002;37(6):631–41.
[12] Ahmad A, Mahanty T, Dubey V, Butola A, Ahluwalia BS, Mehta DS. Effect on the longitudinal coherence properties of a pseudothermal light source as a function of source size and temporal coherence. Opt Lett 2019;44(7):1817–20.
[13] Popescu G. Quantitative phase imaging of cells and tissues. McGraw Hill Professional; 2011.
[14] Dubey V, et al. Partially spatially coherent digital holographic microscopy and machine learning for quantitative analysis of human spermatozoa under oxidative stress condition. Sci Rep 2019;9(1):1–10.
[15] Ahmad A, et al. High-throughput spatial sensitive quantitative phase microscopy using low spatial and high temporal coherent illumination. Sci Rep 2021;11(1):1–13.
[16] Loehrer M, et al. In vivo assessment by Mach–Zehnder double-beam interferometry of the invasive force exerted by the Asian soybean rust fungus (Phakopsora pachyrhizi). New Phytol 2014;203(2):620–31.
[17] Dubey V, et al. Multispectral quantitative phase imaging of human red blood cells using inexpensive narrowband multicolor LEDs. Appl Opt 2016;55(10):2521–5.
[18] Kino GS, Chim SS. Mirau correlation microscope. Appl Opt 1990;29(26):3775–83.
[19] Wang Z, Han B. Advanced iterative algorithm for phase extraction of randomly phase-shifted interferograms. Opt Lett 2004;29(14):1671–3.
[20] Zuo C, et al. Phase aberration compensation in digital holographic microscopy based on principal component analysis. Opt Lett 2013;38(10):1724–6.
[21] Ghiglia DC, Romero LA. Minimum Lp-norm two-dimensional phase unwrapping. J Opt Soc Am A 1996;13(10):1999–2013.